Dentomaxillofacial Radiology (2013) 42, 22027087

http://dmfr.birjournals.org

RESEARCH

Multimodal registration of three-dimensional maxillodental cone beam CT and photogrammetry data over time

N Bolandzadeh*[,1], W Bischof[1], C Flores-Mir[2] and P Boulanger[1]

[1]*Department of Computing Science, University of Alberta, Alberta, Canada;* [2]*Department of Dentistry, University of Alberta, Alberta, Canada*

Objectives: In recent years, one of the foci of orthodontics has been on systems for the evaluation of treatment results and the tracking of tissue variations over time. This can be accomplished through analysing three-dimensional orthodontic images obtained before and after the treatments. Since complementary information is achieved by integrating multiple imaging modalities, cone beam CT (CBCT) and stereophotogrammetry technologies are used in this study to develop a method for tracking *bone*, *teeth* and *facial soft-tissue* variations over time.
Methods: We propose a two-phase procedure of multimodal (Phase 1) and multitemporal (Phase 2) registration which aligns images taken from the same patient by different imaging modalities and at different times. Extrinsic (for Phase 1) and intrinsic (for Phase 2) landmark-based registration methods are employed as an initiation for a robust iterative closest points algorithm. Since the mandible moves independently of the upper skull, the registration procedure is applied separately on the mandible and the upper skull.
Results: The results show that the signed error distributions of both mandible and skull registrations follow a mixture of two Gaussian distributions, corresponding to alignment errors (due to our method) and temporal change over time.
Conclusions: We suggest that the large values among the total registration errors correspond to the temporal change resulting from (1) the effect of treatment (*i.e.* the orthodontic changes of teeth positions); (2) the biological changes such as teeth growth over time, especially for teenagers; and (3) the segmentation procedure and CBCT precision change over time.
Dentomaxillofacial Radiology (2013) **42,** 22027087. doi: 10.1259/dmfr/22027087

Cite this article as: Bolandzadeh N, Bischof W, Flores-Mir C, Boulanger P. Multimodal registration of three-dimensional maxillodental cone beam CT and photogrammetry data over time. *Dentomaxillofac Radiol* 2013; **42:** 22027087.

Keywords: three-dimensional imaging; cone beam computed tomography; photogrammetry; gaussian distribution

Introduction

In recent years, one of the foci of dentistry has been on systems for the evaluation of orthodontic treatments and the tracking of tissue variations in three dimensions over time (also called four-dimensional tracking). Although images obtained from a single three-dimensional (3D) imaging modality [*e.g.* a cone beam CT (CBCT) scanner] may suffice to solve some clinical dental issues, in more general cases, dentists must deal with problems related to multiple body tissues (*i.e.* soft and hard tissues) at the same time. Therefore, it is essential to fuse *multiple* imaging modalities (*e.g.* CBCT and stereophotogrammetry) in order to get complementary information for a complete 3D model of the maxillodental structures and tissues.[1] In this study, we introduce a method for tracking *bone*, *teeth* and *facial soft-tissue* variations of the human head over a long

*Correspondence to: Niousha Bolandzadeh, Aging, Mobility, and Cognitive Neuroscience, 109–828 West 10th Avenue, Vancouver, BC V5Z 1M9, Canada. E-mail: niousha@interchange.ubc.ca
WB and PB were supported by a grant from Natural Sciences and Engineering Research Council of Canada (NSERC).
Received 2 January 2012; revised 12 April 2012; accepted 20 April 2012

period of time, after an orthodontic treatment has been performed. The bone structure of the skull is measured by CBCT modality. For 3D reconstruction of the skin, stereophotogrammetry technology is used.

During the past decade, little research has been conducted on the fusion of CBCT and stereophotogrammetry over time. Integration of CBCT with stereophotogrammetry requires a *registration* procedure, *i.e.* a procedure for spatially aligning two or more images taken from the same patient. The registration can be accomplished on multiple images acquired at different time points before and after the treatments (*i.e.* multitemporal registration) or on images obtained by different modalities of CBCT and 3D photography (*i.e.* multimodal registration). The combination of multitemporal and multimodal registration gives us the ability to make bone and skin evolutions detectable at two different time points (T1 and T2), *e.g.* before and after a treatment.

As an example for multimodal registration, Khambay et al[2] registered 3D images of the skull obtained from CT on the 3D images of the skin obtained from stereophotogrammetry at a single point of time. As an example for multitemporal registration, Cevidanes et al[3] used 3D CBCT images taken before and after orthodontic surgery to assess the mandibular anatomy and position. In another example for multitemporal registration, Kau et al[4] obtained 3D images of the facial soft tissue from a laser scanner before and after orthodontic surgery. Their registration methodology took advantage of the intrinsic facial landmarks, which may have been at risk of changing position during the 6 month scanning process because of tissue swelling. Therefore, one method to overcome this problem could be the combination of multimodal and multitemporal registration. Moreover, this combination gives us the ability to simultaneously track the variations of different body tissues (*e.g.* soft and hard tissues) through time (*i.e.* before and after a treatment).

As far as we are aware, little effort has been made on the combination of multitemporal and multimodal registrations. To the best of our knowledge, the only study capable of tracking soft and hard tissues simultaneously during an orthodontic treatment for long periods of time (*i.e.* greater than 6 months) was a pilot study carried out by Boulanger et al.[5] This study introduced a method for the multimodal and multitemporal registration of CBCT with 3D photography images. However, the investigators did not fully explain the landmarks suitable for multitemporal registration and the procedure of registration over time. Moreover, the method was applied to a single subject, and reliability analysis was not performed.

Owing to the importance of evaluating orthodontic treatments and tracking mandible variations over time, we are introducing a new method for multimodal and multitemporal registrations of data obtained from CBCT and stereophotogrammetry (Figure 1), and we report the validation results.

Materials and methods

Subjects

Six datasets (three females and three males between 10 and 15 years of age at baseline) were chosen from a randomized clinical trial. Three of these datasets were from untreated controls (Subjects 2, 3 and 5), and the other three (Subjects 1, 4 and 6) were from treated patients undergoing a similar orthodontic treatment. Six titanium spheres with a diameter of 6.5 mm were located on a headband placed on the patient's forehead during imaging sessions. Images were obtained in two sessions, before and after the treatment (*i.e.* T1 and T2, respectively), within an 8–12 month period. For each subject, images of CBCT and stereophotogrammetry were acquired almost simultaneously at each visit at times T1 and T2. Informed consent and ethical approval for the study was granted by the University of Alberta Health Research Ethics Board (#5835), Alberta, Canada.

Bone acquisition and pre-processing procedure

A NewTom QR-DVT9000 CBCT scanner (Aperio Services, Verona, Italy) set at 110 kV, 6.19 mA, 8 mm aluminium filtration, 12 inch field of view, and slice thickness of 0.5 mm was used to acquire the 3D skull and teeth structures of the patient lying in a supine position. In our experiments, we relied on the machine setting to set the dose to the patient to standard safe values. The effective dose could be estimated approximately based on the studies of Lorensen and Cline[6] and Erem and Dedual,[7] but they are problematic as CBCT manufacturers claim to the dose is significantly reduced compared with normal CT. There is a direct link between beam intensity and the quality of the geometry produced by the marching cubes algorithm. A higher beam brightness does produce a better image and hence a better geometry. In many ways, the real question is: what is the minimal beam brightness setting that is sufficient to produce accurate geometry that can be used for comparison? For our 3D CBCT images, a marching cubes algorithm[6] with an isodensity value of 950 was used to extract the skull geometry from the CBCT density values. This value was determined manually such that it led to an optimal segmentation of bone from the soft tissue. The marching cubes[6] algorithm is an interactive segmentation algorithm that uses a user-defined threshold to produce polygonal triangle meshes of constant density surfaces (*i.e.* equal to the isosurface value) from 3D data.[7] As a consequence, different surfaces such as the skull can be extracted from a 3D volume density model. In addition to the marching cubes algorithm, a decimating filter[8] (set at 80%) was applied to reduce the number of triangles produced from the marching cubes algorithm. This decimation is essential, as large polygon counts are hard to process and cannot be displayed easily in real time. CBCT scanners suffer from precision change that is further explained in the Discussion. Figure 2 shows a polygonal skull constructed from this procedure.

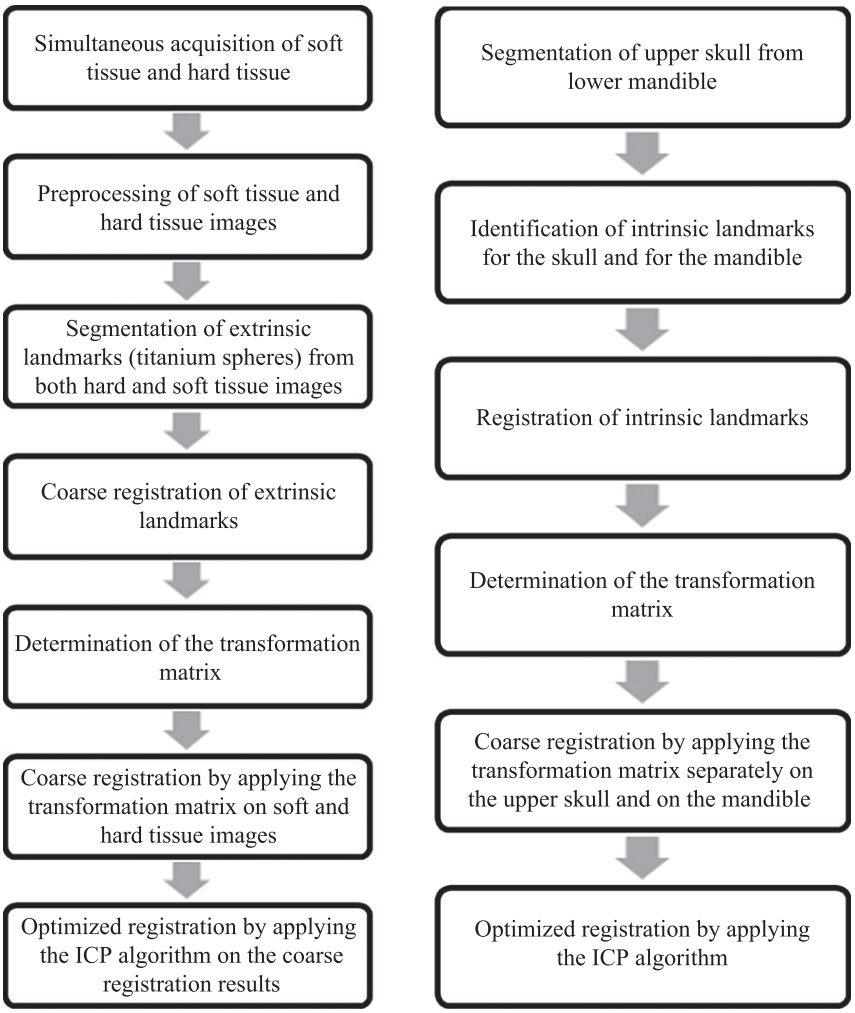

Figure 1 Flowchart of the proposed registration methodology. Phase 1 is illustrated on the left and Phase 2 is illustrated on the right. ICP, iterative closest points

Skin acquisition and pre-processing procedure

A 3dMDface system (3dMD, Atlanta, GA) was mounted on top of the NewTom CBCT device. The patient was in a supine position for both imaging intakes. Furthermore, the hard- and soft-tissue acquisitions were consecutive but without the patient moving from the supine position. So, the position of the mandible stayed the same for both 3D photography and CBCT.

The 3dMDface system consists of six cameras and four flash units. Two infrared cameras, one speckle flash unit, one texture flash unit and one colour camera, are mounted on each side of the device. By combining the natural facial patterns with projected unstructured light, the geometry of the face is captured by the cameras.[9] A triangulation algorithm uses the light projection information combined with natural patterns of the skin to build the geometric 3D meshes of the face. The colour information captured by the colour cameras is then mapped on the surface after the mesh reconstruction. The result is a textured polygonal structure with approximately 50 000 triangles. Figure 3 shows the polygonal face constructed using the 3dMD scanner.

Registration methods

Registration is the process of spatially aligning two or more images obtained from the same subject. Multimodal registration takes images from different sensors (*e.g.* CT and photogrammetry), and multitemporal registration takes images from different time points (*e.g.* before and after the treatment). A complete and simultaneous tracking of the shape variations for the head skin and bone structures necessitates a multimodal and multitemporal registration of CBCT and stereophotogrammetry data obtained at different times.

In this study, the registration procedure is divided into two phases. The first phase consists of performing the multimodal registration of the CBCT and the stereophotogrammetry data at each time point. The second phase uses the results of the first phase (saved as

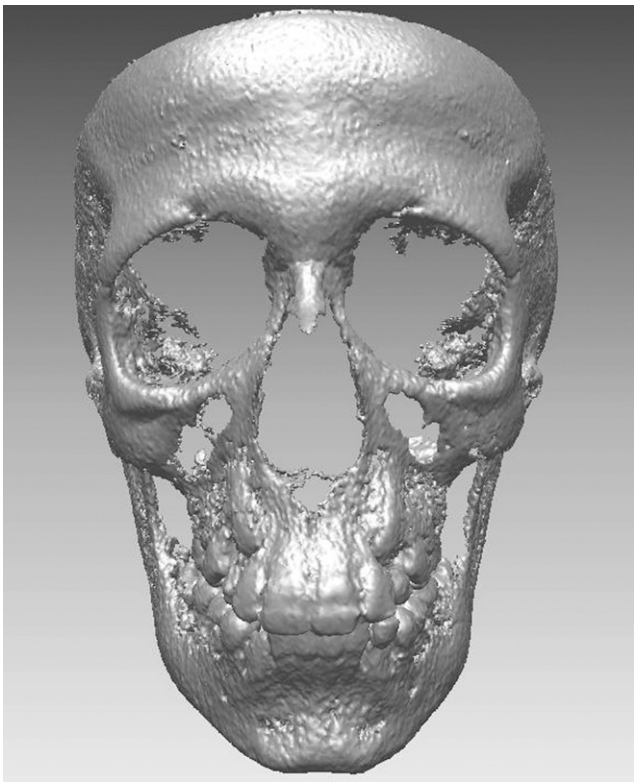

Figure 2 Three-dimensional reconstruction of the skull from cone beam CT using a NewTom scanner

Figure 3 Three-dimensional reconstruction of the skin from stereophotogrammetry using a 3dMD face scanner

a polygonal shell for T1 and T2 separately) to group the registered polygons into a common coordinate system.

In this sense, for the first phase, an extrinsic landmark-based registration method was applied to the multimodal CBCT and stereophotogrammetry data separately for each visit. For the second phase, an intrinsic landmark-based registration method was used for single-modal multitemporal CBCT data of the skull and the mandible, between T1 and T2 visits. The combination of multimodal and multitemporal registration methods provided us with one 3D model, consisting of the skin and the skull images from different time points registered altogether.

Phase 1: multimodal registration of CBCT and stereophotogrammetry. Extrinsic landmark-based registration was used for the multimodal registration of CBCT and stereophotogrammetry data at each time point. This registration method relies on the artificial landmarks to find the optimal geometric transformation between modalities. It is necessary to have extrinsic landmarks that do not scatter the radiation beam and are clearly identifiable in both modalities. Therefore, six titanium spheres glued on a headband were used as extrinsic landmarks.

To register the CBCT and stereophotogrammetry geometries, we started by first registering the extrinsic landmarks pairwise, by using a mean square sphere-fitting routine with a fixed radius of 3.25 mm, capable of performing automatic outlier detection. From the fitted spheres, the estimated centres were taken as the reference points for datasets to be registered. Figure 4 shows the virtual spheres fitted on the headbands' spheres, for both the stereophotogrammetry and the CBCT datasets.

After finding each reference sphere's centre, a transformation matrix was found between the nearest points using a point registration routine. The coarse registration result was then used as a starting point for an iterative closest point (ICP) algorithm.[10] In fact, the landmark-based algorithm served only as an initiation step for our main registration algorithm (*i.e.* ICP). The ICP algorithm iteratively tries to minimize the cost function (*i.e.* sum of the squared distances between two shells) over all the possible transformations consisting of translations and rotations. This method is guaranteed to converge to a local minimum.[11] In this study, the maximum average for deviations was set to 1 mm for the ICP algorithm. This parameter is set to eliminate outliers, which, as described by Rusinkiewicz and Levoy,[12] is essential when ICP is performing a least-squares minimization. The result of multimodal registration of the skin and the skull is presented in Figure 5.

Phase 2: multitemporal registration between visits. Once the multimodal data are registered separately for each visit at times T1 and T2, the polygon set (*i.e.* the integrated skin and skull) from T1 should get registered with the one at time T2. The challenge of this process is that it is impossible to guarantee that the extrinsic landmarks are located at the same place on different

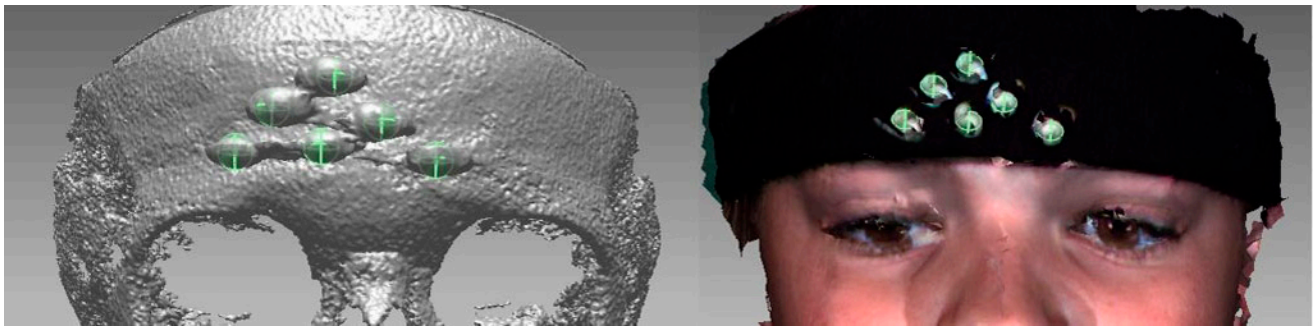

Figure 4 Virtual spheres fitted on the physical titanium spheres attached to the headband. The left figure shows the spheres on the skull, and the right figure shows the spheres on the skin. These fitted spheres are used as extrinsic landmarks for the multimodal registration of stereophotogrammetry and cone beam CT data. Note that the shapes of titanium spheres are distorted due to beam hardening on the left figure. However, this beam hardening effect had limited impact on the sphere-fitting process as we were using a robust fitting algorithm with automatic outlier detection. In most cases, the influence of this distortion on some of the points was eliminated

visits. The shape of the subject's face and lower jaw may not be the same, as a result of normal growth and development changes or orthodontic treatment effects. Therefore, we used *intrinsic anatomical* landmarks for multitemporal registration.

Since the mandible moves independently of the upper skull, it should be analysed separately. Therefore, for each skull in T1 and T2, the mandibles were segmented manually from the upper skull and intrinsic anatomical landmarks were selected for each section separately (Figures 6 and 7).

The skull landmarks (Figure 6) were selected since they are believed to be stable over long periods and are easily identifiable at different times. Moreover, as suggested by Nielsen et al,[15] for registration of time sequence images of the mandible, nerve passage foramina and the inner cortical surfaces were selected as the intrinsic landmarks (Figure 7).

Once the points were selected on the CBCT data, the transformation matrix between the intrinsic landmarks was found by a landmark-based registration algorithm, and the two skulls were registered. By applying the same transformation to the entire polygon shell, the stereophotogrammetry skin data, which had been registered with CBCT data in Phase 1, was also registered. From the initial estimate of the landmark registration, a robust ICP algorithm was then used to optimize the quality of the registration. A robust ICP algorithm is capable of automatically performing outlier detection, eliminating pairings that are greater than the average distances between points.

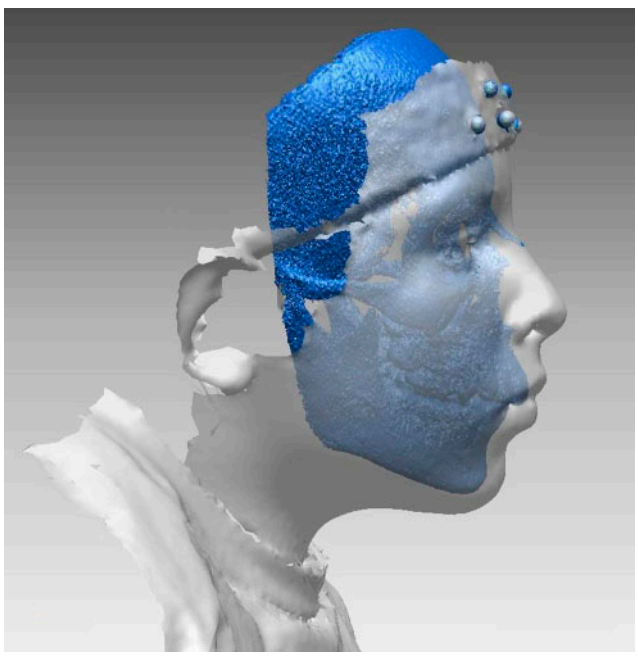

Figure 5 Final result of multimodal registration of the skull and the skin using extrinsic landmarks (titanium spheres) shown on the patient's forehead. The inner shell represents the skull, and the outer shell represents the skin

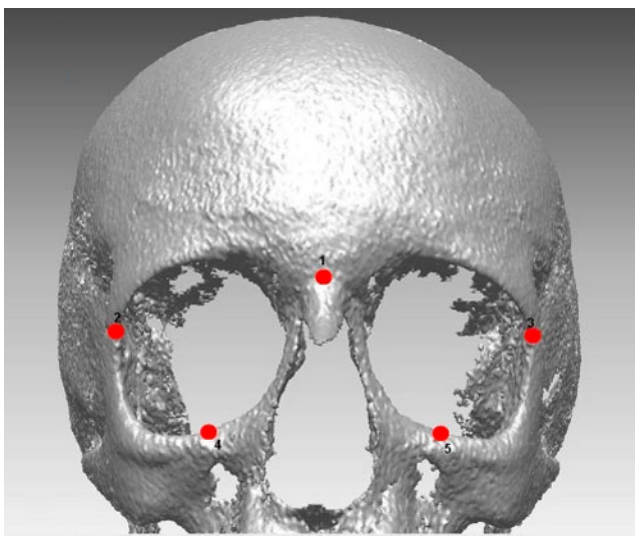

Figure 6 Five anatomical skull landmarks used for multitemporal registration of cone beam CT data, from T1 to T2. These landmarks are easily identifiable through X-ray images and are relatively stable through time

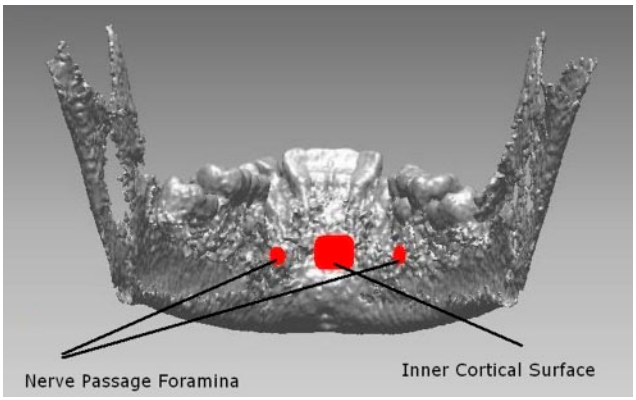

Figure 7 Three anatomical mandible landmarks used for multi-temporal registration of cone beam CT data, from T1 to T2. These landmarks are easily identifiable through X-ray images and are relatively stable through time

Experimental results and registration validation

To evaluate our registration results, the registration errors were defined as the signed distances (in millimetres) between the nearest points of registered T1 and T2 shells. As a result, the distances of T1 data points were measured from their closest triangles in corresponding T2 shells along with a positive or negative sign due to the position of the point relative to the triangle normal (inside or outside). The registration errors were measured separately for skulls and mandibles.

Based on the central limit theorem, we expected our signed distances to follow a gaussian (normal) distribution if there was no bias involved in the registration process. In this regard, any misregistered data create an error distribution that does not follow the gaussian assumption. Moreover, since the images were taken at different times and under different conditions, the signed distances should be clustered into two different components, one component due to the alignment (*i.e.* related to our method) errors, and the other due to the temporal change (*i.e.* treatment and facial growth, which we cannot discriminate). To achieve this, a k-means clustering algorithm was used to partition the data into two clusters. This algorithm partitioned the data into two ($k = 2$) clusters in which each data point belonged to the cluster with the nearest mean. Expectation maximization (EM) was then used to fit a gaussian mixture model to the signed distances. For each of the clusters, this algorithm iteratively tried to find the maximum likelihood of parameters for normal distributions. These estimated parameters were then used to partition the data into two clusters, whose Gaussian probability distribution functions were estimated and plotted.

Figures 8 and 9 show the Gaussian mixture models for a skull (Figure 8) and a mandible (Figure 9) for one subject. The Gaussian model plotted in dotted format represents the distribution of the alignment errors, whereas the Gaussian distribution plotted in triangle format represents the distributions of the temporal change. The sum of the two Gaussian probability distribution functions is also plotted in regular line format.

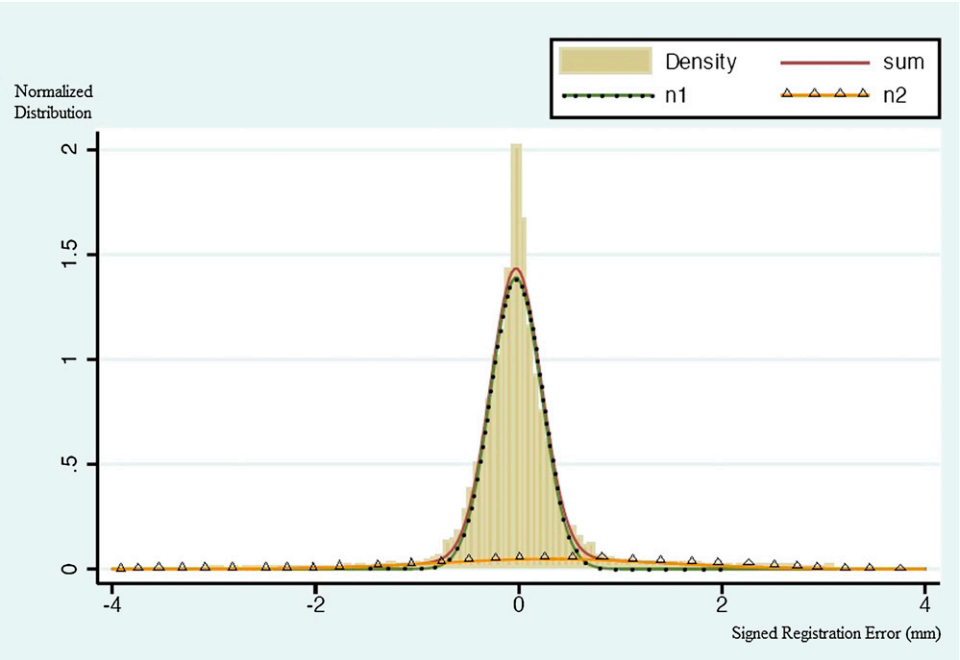

Figure 8 A gaussian mixture model of two components fitted on the skull data. The n1 plots represent the distribution of the alignment errors, whereas the n2 gaussian distributions represent the temporal change. As presented, the distribution of the temporal change has a larger mean and standard deviation than the alignment errors. This shows that a larger portion of the total registration errors is due to the temporal change, and not our proposed method errors (*i.e.* the alignment errors)

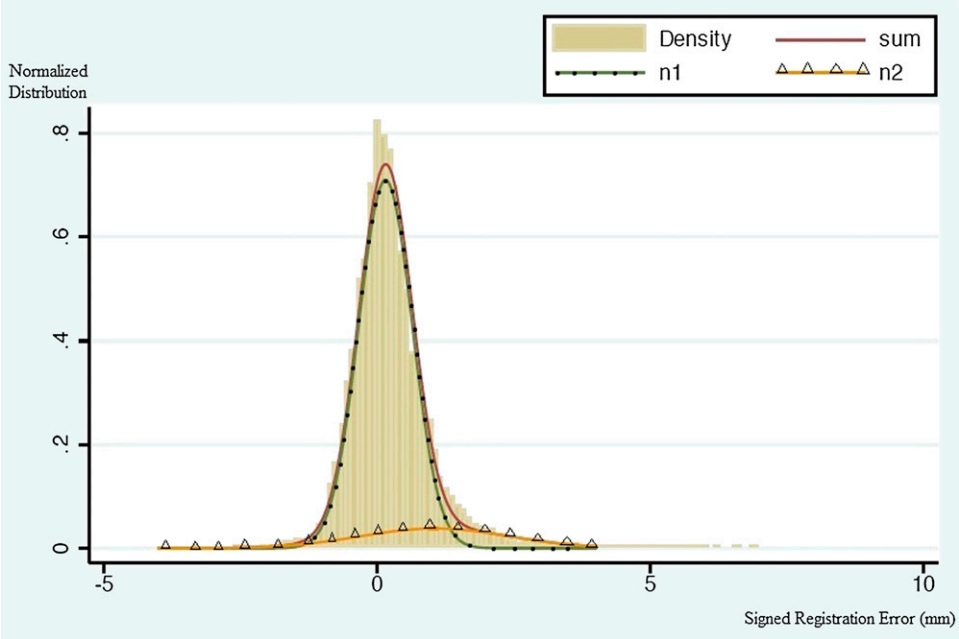

Figure 9 A gaussian mixture model of two components fitted on the mandible data. The n1 plots represent the distribution of the alignment errors, whereas the n2 gaussian distributions represent the temporal change. As presented, the distribution of the temporal change has a larger mean and standard deviation than the alignment errors. This shows that a larger portion of the total registration errors is due to the temporal change, and not our proposed method errors (*i.e.* the alignment errors)

The parameters of both Gaussian components, the alignment and temporal change, are given in Table 1. As shown, the estimated temporal change is much larger than the estimated alignment errors, for both skull and mandible. The average ratio of the standard deviations of temporal change over alignment errors is 3.38 mm for the mandibles, and 3.41 mm for the skulls. These ratios along with larger measurements for all the estimated *temporal change* compared with their corresponding alignment errors suggest that the large values (*i.e.* the outliers) among the total registration errors are due to temporal change, not alignment errors. Therefore, the small error values associated with our registration method (*i.e.* the alignment error) are representative of the high accuracy of the registration method for this study.

Moreover, one does not always need an external reference shape to validate registration and confirm how well the registration works. In an ideal world this could be done. However, in clinical applications this is not necessary, as during registration we are using the upper part of the skull as a reference with the realistic assumption that the upper skull does not change in the time period we are dealing with. Second, we are performing an outlier diagnostic before the final registration to make sure the outliers (points that have moved significantly during the time period) do not interfere with the final mean square registration with all the inlier points. This is an accepted practice in industrial metrology and is used to validate aeroplane wings to car parts. The fact that the difference of the large majority of points between the two skulls follows an unskewed Gaussian distribution is strong evidence that the registration does not have a systematic bias. Furthermore, the fact that the variance falls into the known precision of CBCT (0.3 mm) is also evidence that the registration is good and the skull stability assumption is valid.

Table 1 The normal distribution functions [formulated as N (mean, standard deviation^2)] estimated for alignment errors and temporal change, extracted from the skull and the mandible signed errors

Subjects	*Mandible alignment error*	*Temporal change (between T1 and T2)*	*Skull alignment error*	*Temporal change (between T1 and T2)*
Subject 1 (treated)	N (0.0032, 0.4444^2)	N (1.1799, 1.2044^2)	N (0.3772, 0.3175^2)	N (0.3772, 1.0251^2)
Subject 2 (control)	N (0.1510, 0.4871^2)	N (1.7621, 1.4257^2)	N (0.1606, 0.5205^2)	N (2.2225, 2.1840^2)
Subject 3 (control)	N (−0.0978, 0.4287^2)	N (0.0562, 1.3843^2)	N (−0.0177, 0.3289^2)	N (0.2161, 1.4472^2)
Subject 4 (treated)	N (−0.4517, 0.4891^2)	N (−1.3552, 1.4725^2)	N (−0.4768, 0.4802^2)	N (−0.4999, 1.6201^2)
Subject 5 (control)	N (0.0274, 0.4687^2)	N (1.1949, 1.6749^2)	N (0.0044, 0.2432^2)	N (0.4418, 1.6285^2)
Subject 6 (treated)	N (−0.1342, 0.4920^2)	N (1.1270, 2.3895^2)	N (−0.0273, 0.2521^2)	N (0.5246, 1.3304^2)

All measurements are in millimetres.

Discussion

Integrating multiple 3D imaging modalities in dentistry gives us the ability to reconstruct different tissue types (*e.g.* bone, teeth and facial soft tissue) and visualize 3D models of the patients. The information obtained from the reconstruction of different tissues in 3D, before and after a treatment, may help to quantify patient outcomes, which may result in the development of better treatments and more objective surgical planning. The proposed method is in the interest of manufacturers too, as they are interested in making multimodal registrations easier.[13]

In this study, we introduced a method for tracking bone, teeth and facial soft-tissue variations over a 1 year period of time. Because complementary information can be achieved from multiple modalities, CBCT and 3D photography technologies were used to reconstruct bone and skin structures of the face. Six subjects, including three subjects experiencing a treatment and three untreated controls, underwent the data acquisition process at two different points of times (T1 and T2), within an 8–12 month period.

Comparing 3D models of the skull with the skin captured at one point of time gives us the ability to analyse the effects of bone variations on the skin structure. Moreover, comparing skull and skin variations before and after a treatment may help physicians to evaluate treatment results. As a consequence, a registration procedure is needed in order to overlay 3D skin over 3D skull models at each point of time and between visits, before and after the treatment. Our proposed tracking system consists of a two-phase registration procedure. In the first phase, we extracted from both modalities extrinsic landmarks which were put on the subject's forehead during the imaging sessions, and registered them using a 3D rigid registration algorithm. As a result of this registration methodology, one can analyse the effects of bone treatments on the facial soft tissue. In the second phase of registration, we took advantage of intrinsic landmarks on the skull geometry at times T1 and T2 to apply an automatic, robust registration algorithm. The skeletal anatomical landmarks were chosen from those which could be easily identified, and did not change or grow during the interval of T1 to T2. Since the mandibles can move independently of the upper skulls and therefore should be registered separately for specific clinical questions, the same registration procedure with mandible intrinsic landmarks (also easily identifiable and relatively stable through time) was performed on the mandibles after they were segmented from the upper skull.

We validated our method by fitting a Gaussian mixture model (with two components) to the registration errors. These Gaussian distributions can be classified as alignment errors and temporal change. We suggest that the small values among the total registration errors are due to our proposed registration method (*i.e.* alignment errors). The large values among the total registration errors (*i.e.* temporal change) are outliers and have several possible causes. First, the effect of treatment (*i.e.* the orthodontic changes in the position of patients' teeth) may have influenced the measured distances between T1 and T2. Second, they may be caused by biological changes such as tooth growth from T1 to T2. A big portion of the calculated large deviations were due to the eruption of teeth from T1 to T2, especially for teenagers. Third, the segmentation procedure, *i.e.* the extraction of skull structure from the CT density data, may have resulted in different meshes for T1 and T2, even with the same scanning parameters. This segmentation error that might be due to the CT intensity calibration could yield large outliers if the scanning parameters were not tightly controlled. Moreover, the pre-set thresholds for bones using Hounsfield units are not accurate (as CBCT machines do not provide Hounsfield units in the sense of relatively accurate density values, in contrast to CT machines), and the precision change over time as the machine thermal equilibrium is reached during the day.[14]

In conclusion, our method produces alignment results of high accuracy and can thus be employed by dentists and physicians for tracking treatment results. We believe that a main source of outliers in our registration method is caused by segmentation. Further investigations on the effects of different isosurface values of the marching cubes algorithm may result in finding optimized values for registration. Finally, the development of an automatic process for the segmentation of mandibles, as well as automation of anatomical landmark detection may help to further reduce the temporal change, and therefore to further improve the registration results.

References

1. Azhari H, Edelman RR, Townsend D. Multimodal imaging and hybrid scanners. *J Oral Maxillofac Surg* 2004; **62**: 1497–1504.
2. Khambay B, Nebel JC, Bowman J, Walker F, Hadley DM, Ayoub A. 3D stereophotogrammetric image superimposition onto 3D CT scan images: the future of orthognathic surgery. A pilot study. *Int J Adult Orthodon Orthognath Surg* 2002; **17**: 331.
3. Cevidanes LH, Bailey LJ, Tucker GR Jr, Styner MA, Mol A, Phillips CL, et al. Superimposition of 3D cone-beam CT models of orthognathic surgery patients. *Dentomaxillofac Radiol* 2005; **34**: 369.
4. Kau CH, Cronin A, Durning P, Zhurov AI, Sandham A, Richmond S. A new method for the 3D measurement of post-operative swelling following orthognathic surgery. *Orthod Craniofacial Res* 2006; **9**: 31–37.
5. Boulanger P, Flores-Mir C, Ramirez JF, Mesa E, Branch JW. Long term three dimensional tracking of orthodontic patients using registered cone beam CT and photogrammetry. Conf Proc IEEE Eng Med Biol Soc 2009: 3525–8.

6. Lorensen WE, Cline HE. Marching cubes: a high resolution 3D surface construction algorithm. *ACM Siggraph Computer Graphics* 1987; **21**: 163–169.
7. Erem B, Dedual N. Surface construction analysis using marching cubes. Northeastern University; 2009. pp 8–12. Available from: http://www.ndedual.com/wp-content/uploads/marchingcubes.pdf
8. Schroeder WJ, Zarge JA, Lorensen WE. Decimation of triangle meshes. *Computer graphics—new york association for computing machinery* 1992; **26**: 65–70.
9. Lane C, Harrell W, Jr. Completing the 3-dimensional picture. *Am J Orthod Dentofacial Orthop* 2008; **133**: 612–620.
10. Besl PJ, McKay ND. A method for registration of 3-D shapes. *IEEE Trans Pattern Anal Mach Intell* 1992; **14**: 239–256.
11. Chui H, Rangarajan A. A new point matching algorithm for non-rigid registration. *Comput Vis Image Underst* 2003; **89**: 114–141.
12. Rusinkiewicz S, Levoy M. *Efficient variants of the ICP algorithm*. Proceedings of the Third International Conference on 3D Digital Imaging and Modeling, 2001; 28 May–1 June 2001; Quebec City, Canada. Washington DC: IEEE Computer Society, 2001.
13. Planmeca. [cited 8 March 2012] Available from: http://www.planmeca.com/en/imaging/3d_imaging/planmeca_proface.
14. Logan HA. *Utility of digital surgical simulation planning and solid free form modeling in fibula free flap mandibular reconstruction*. Master's thesis. Ednonton: University of Alberta; 2012.
15. Bio-Nielsen M, Gramkow C, Kreiborg S. Non-rigid image registration using bone growth model. In: Troccaz J (ed.). CVRMed–MRCAS 1997, Lecture Notes in Computer Sciences. New York City, NY: Springer; 1997. pp. 1–12.